Chain Localization and Interfacial Thickness in Microphase-Separated Structures of Block Copolymers with Variable Composition Distributions

Atsushi Noro,[†] Masatoshi Okuda,[†,§] Fumitake Odamaki,[†,⊥] Daisuke Kawaguchi,[†] Naoya Torikai,[‡] Atsushi Takano,[†] and Yushu Matsushita*[,†]

Department of Applied Chemistry, Graduate School of Engineering, Nagoya University, Furo-cho, Chikusa-ku, Nagoya 464-8603, Japan, and Neutron Science Laboratory, High Energy Accelerator Research Organization, 1-1 Oho, Tsukuba, Ibaraki 305-0801, Japan

Received July 3, 2006; Revised Manuscript Received August 24, 2006

ABSTRACT: The effect of composition distribution on microphase-separated structures of AB diblock and BAB triblock copolymers was investigated at the molecular level by measurements of neutron reflectivity. Monodispersed three poly(styrene)-d_8-*block*-poly(2-vinylpyridine) (DP) and three labeled triblock copolymers (PDP) and unlabeled counterparts were synthesized by a living anionic polymerization process designed to yield constant molecular weight with different volume fractions. The selective labeling method employs the blending of copolymers for a segmental distribution study while the labeled polymers are mixed for an interfacial study. Scattering length density profiles were observed by neutron reflectivity measurements for blended thin films produced by spin-coating and successive thermal annealing. It was confirmed that the blended thin films exhibit simple alternating lamellar structures, an observation consistent with the observed structures of bulk specimens. The localization phenomenon of longer and shorter block chains was also investigated. Longer block chains are generally localized at the center of the domains while the shorter block chains are localized near the domain interface as suggested by previous morphological observations. Interfacial thickness increases with an increase in composition distribution index for both diblock and triblock systems. The incremental increase for the triblock system is larger than that of the diblock system.

Introduction

Morphologies of block copolymers have been theoretically and experimentally studied for nearly four decades.[1−10] Molecular weights and compositions are parameters that have been extensively investigated. Several studies of block copolymers employed AB diblock copolymers to take advantage of their basic chemical structures,[3−5,11] although block copolymers with complex chemical structures have also been systematically investigated.[12−16] BAB-type triblock copolymers have been extensively studied. These polymers adopt both bridge and loop conformations because their midblocks lack chain ends.[12,14,17,18]

Studies of samples produced by systematic blending were also performed for AB diblock copolymer/A homopolymer blends[19−22] and for AB diblock copolymer/AB diblock copolymer blends.[23−26] The block copolymer samples used in these studies have narrow distributions of compositions and molecular weights because these parameters are thought to affect the morphologies and properties of block copolymers. Block copolymers used in industry, however, generally possess wide distributions of compositions and molecular weights, and the effects of these two parameters have not been separately evaluated.[27]

We have recently succeeded in quantitatively evaluating the dependence of composition distribution and molecular weight distribution on microphase-separated structures formed by polystyrene-*block*-poly(2-vinylpyridine) (SP) diblock copolymers and poly(2-vinylpyridine)-*block*-polystyrene-*block*-poly(2-vinylpyridine) (PSP) triblock copolymers by blending several monodispersed samples.[28−31] Related investigations have been undertaken by others.[32−39] Our investigations indicated that SP and PSP block copolymers with an average S/P volume ratio of 0.5/0.5 for two different distribution systems exhibit simple and periodic lamellar structures when the polydispersity indices of samples are lower than the critical value and that lamellar domain spacing increases with an increase in polydispersity indices of the blends. These results led us to propose that the microdomain expansion may be caused by the localization of long block chains in lamellar microdomains since nonuniform distributions of component polymers, particularly those of longer chains, were observed for ordered binary block copolymer blends as demonstrated by Mayes et al.[26] Moreover, domain expansion behavior was observed for block copolymer/homopolymer blend systems where homopolymer chains were localized in microdomains.[19−22] Neutron reflectivity (NR) measurements[40] have indicated that partial segments near the junction points are localized at the domain interface while the free ends are localized at the domain center.[41−43]

NR profiles are also known to contain information about interfacial thickness. As stated above, bulk domain spacing for polydispersed block copolymer systems is larger than that of monodispersed systems, while it is unknown whether or not polydispersity of block chains influences interfacial structure. If interfacial thickness depends on the polydispersity of the system, this relationship would be of great interest because it could affect the miscibility of incompatible polymers.[41,42] Although theoretical studies on the polydispersity of immiscible polymers such as the work of Shi et al. have been carried out,[44,45] experimental investigations have not yet been pursued.

* Corresponding author: Phone +81-52-789-4604; Fax +81-52-789-3210; e-mail yushu@apchem.nagoya-u.ac.jp.
† Nagoya University.
§ Present address: Ibiden Co. Ltd.
⊥ Present address: Fuji Heavy Industries Ltd.
‡ High Energy Accelerator Research Organization.

10.1021/ma061487k CCC: $33.50
Published on Web 10/06/2006

Table 1. Molecular Characteristics of Parent Diblock Copolymers

sample	M_w[a]/10^5	M_w/M_n[b]	ϕ_S[c]	M_w(S)[d]/10^4
DP-19	1.44	1.02	0.100	1.43
DP-55	1.24	1.02	0.503	6.21
DP-91	1.15	1.03	0.911	10.5
SP-19	1.05	1.03	0.100	0.975
SP-55	1.35	1.04	0.462	5.96

[a] Weight-averaged molecular weights measured by multiangle laser light scattering. [b] Apparent polydispersity indices measured by gel permeation chromatography. [c] Volume fractions of polystyrene blocks measured by pyrolysis−gas chromatography. [d] Molecular weights of polystyrene blocks calculated by using M_w, ϕ_S, and bulk densities of component polymers, i.e., 1.05 for polystyrene-h_8, 1.13 for polystyrene-d_8, and 1.14 for poly(2-vinylpyridine).

Table 2. Molecular Characteristics of Parent Triblock Copolymers

sample	M_w[a]/10^5	M_w/M_n[b]	ϕ_S[c]	M_w(S)[d]/10^4
PDP-28	1.19	1.05	0.249	2.94
PDP-55	1.43	1.04	0.469	6.68
PDP-82	1.44	1.05	0.758	10.9
PSP-28	1.58	1.07	0.224	3.32
PSP-55	1.56	1.05	0.496	7.42

[a −d]The meaning of all values are the same as those in Table 1.

In the present work, the microdomain structures of blended samples with wide composition distributions were investigated at the molecular level by neutron reflectivity to observe the localization phenomena of block chains with different chain lengths. Interfacial thickness was also measured. A selective labeling method was employed for the localization study while blends having two different composition distribution indices were prepared for the interfacial study by mixing deuterium-labeled parent copolymers and retaining an average S/P (0.5/0.5) volume ratio and a constant average molecular weight.

Experimental Section

All deuterated parent block copolymers, i.e., three poly(styrene)-d_8-*block*-poly(2-vinylpyridine) (DP) diblock copolymers and three poly(2-vinylpyridine)-poly(styrene)-d_8-*block*-poly(2-vinylpyridine) (PDP) triblock copolymers, were synthesized in tetrahydrofuran (THF) at −78 °C by a sequential living anionic polymerization process using cumyl potassium and naphthalene potassium as initiators, respectively.[30] These copolymers were purified by reprecipitation in hexane and dried in vacuo. Freeze-drying was then carried out to remove remaining solvents.

Gel permeation chromatography was performed to measure polydispersity indices using the HLC-8020 (GPC) system (Tosoh Corp.) with three G4000H columns. Absolute weight-averaged molecular weights of parent block copolymers were determined by multiangle laser light scattering (MALLS) using the DAWN EOS enhanced optical system (Wyatt Technology).[30] Volume fractions of the polystyrene block for all block copolymers were measured by pyrolysis−gas chromatography (pyrolysis−GC), using a Shimadzu GC-2010 equipped with a PY-2020s pyrolyzer (Frontier Laboratory) with an ultra-alloy column and an FID detector as described previously.[30]

Tables 1 and 2 exhibit molecular characteristics of all parent block copolymers used in this study for the diblock and triblock systems. The molecular weights of all copolymers are close to 130K, and their polydispersity indices are all less than 1.07. Volume fractions of the polystyrene block, ϕ_S, for the three DP diblock copolymers are approximately 0.1, 0.5, and 0.9, while the volume fractions of the PDP triblock copolymers are approximately 0.2, 0.5, and 0.8. Since a given triblock copolymer with a broad composition distribution tends toward separation of macrophases,[28,29] the volume fraction gap between the smallest parent copolymer and the largest parent copolymer for the triblock system was designed to be smaller than that of the volume fraction gap of the diblock system. Two unlabeled SP diblock copolymers having

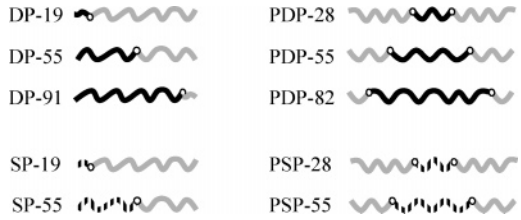

Figure 1. Schematic representations of all parent block copolymers used in this study. Black chains, broken-line chains, and gray chains represent polystyrene-d_8, polystyrene-h_8, and poly(2-vinylpyridine), respectively.

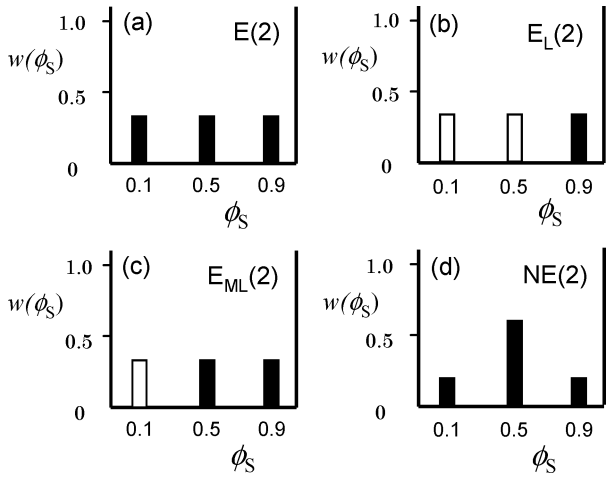

Figure 2. Blend characteristics of parent diblock copolymers: (a) **E(2)**, (b) $\mathbf{E_L(2)}$, (c) $\mathbf{E_{ML}(2)}$, and (d) **NE(2)**. The horizontal axes represent polystyrene volume fractions of the parent copolymers. The vertical axes represent weight fractions. The white bars indicate unlabeled SP diblock copolymers. The black bars represent deuterium-labeled DP diblock copolymers.

polystyrene content of approximately 0.1 and 0.5 and two earlier synthesized unlabeled PSP triblock copolymers with ϕ_S of approximately 0.2 and 0.5 are also listed in Tables 1 and 2. Schematic illustrations and code names of all parent block copolymers used are shown in Figure 1. The perdeuterated polystyrene block chains are illustrated with black bars.

The blended samples of the diblock and triblock copolymers were prepared using three different parent block copolymers with different volume fractions out of five in Tables 1 and 2, respectively. For all blend samples, the weight fractions of the two parent copolymers with the smallest and the largest ϕ_S were set as equal to retain a constant ϕ_S value of 0.5. With this condition, four blend samples were prepared for the diblock and triblock systems.

Figure 2 shows the blend characteristics of the diblock system as an example, where the horizontal axes represent polystyrene content, ϕ_S, of parent block copolymers and the vertical axes represent the weight fractions, $w(\phi_S)$, of blended parent block copolymers. Figure 2a represents an equal mass fraction blend from three deuterium-labeled parent diblock copolymers (**E(2)**). This blend has two derivatives. The first one, $\mathbf{E_L(2)}$ as shown in Figure 2b, includes a labeled long polystyrene chain and two additional unlabeled chains for the purpose of determining the segmental distribution of the long block chain, while $\mathbf{E_{ML}(2)}$ in Figure 2c includes labeled medium and long chains with an unlabeled short chain for the purpose of determining the segmental distribution of an unlabeled short block chain. Blend characteristics are similar to those employed by Mayes et al.[26] in view of selective labeling of block chains, but different with regard to retaining constant molecular weight and composition. On the other hand, Figure 2d indicates the symmetric but nonequal distribution of three deuterium-labeled parent copolymers, **NE(2)**, to investigate the effects of composition distribution on interfacial thickness. These three copolymers were designed to have weight fraction ratios of 1:3:1. Successively, the same rationale was employed in the preparation

Table 3. Codes and Characteristics of Blend Samples

code	$M^a/10^5$	M_w/M_n(block)^b	$\phi_S{}^c$	D_{SAXS}/nm	D_{NR}/nm	$t_I{}^d$/nm
DP-55	1.24	1.02	0.503	56.1	56.6	3.3 ± 0.3
NE(2)	1.26	1.28	0.504	60.3	60.8	3.8 ± 0.3
E(2)	1.27	1.46	0.505	64.2	64.7	4.0 ± 0.3
$E_L(2)$	1.17	1.44	0.491	64.3	64.8	
$E_{ML}(2)$	1.14	1.43	0.505	62.5	63.0	
PDP-55	1.43	1.04	0.469	37.6	38.1	3.2 ± 0.3
NE(3)	1.38	1.11	0.483	38.8	36.9	3.8 ± 0.3
E(3)	1.34	1.18	0.492	38.8	36.5	4.0 ± 0.3
$E_L(3)$	1.52	1.20	0.493	40.4	40.9	
$E_{ML}(3)$	1.48	1.20	0.483	39.4	39.9	

[a] The calculated average molecular weights using M_w values in Tables 1 and 2. [b] Composition distribution indices calculated according to the definition $\{M_w(S)/M_n(S) + M_w(P)/M_n(P)\}/2$ for all blends. [c] Volume fractions of polystyrene blocks estimated by using ϕ_S values in Tables 1 and 2. [d] Interfacial thicknesses determined by neutron reflectivity measurements.

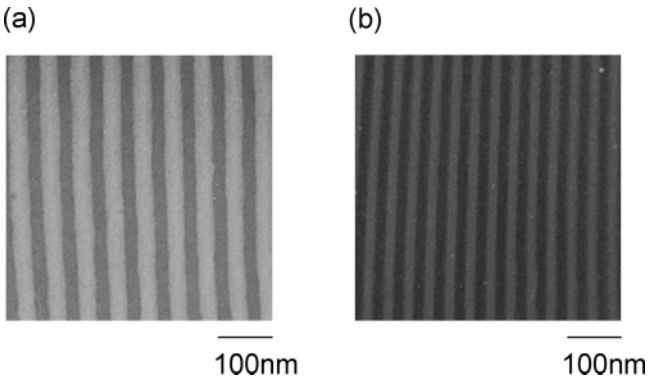

Figure 3. Typical transmission electron micrographs of the blend **E**s for the diblock and triblock systems: (a) **E(2)** blend; (b) **E(3)** blend. The light domain represents the polystyrene phase, and the darker domain represents the poly(2-vinylpyridine) phase. Sample specimens were stained with osmium tetroxide.

of a triblock copolymer system and four blends, i.e., **E(3)**, $\mathbf{E_L(3)}$, $\mathbf{E_{ML}(3)}$, and **NE(3)**.

Table 3 compares the characteristics of blend samples. The polydispersity of parent block copolymers was assumed to be unity for calculation of overall "composition distribution" indices, defined as the arithmetic averages of molecular weight distribution indices of both component blocks as follows:

$$M_w/M_n(\text{block}) = \{M_w(S)/M_n(S) + M_w(P)/M_n(P)\}/2$$

where $M_w(X)$ = weight-average and $M_n(X)$ = number-average molecular weights of component block X (where X denotes S or P) in copolymers.[30] Because the S and P blocks in our blend samples have almost the same composition, i.e., S/P = 0.5/0.5, we employ simple arithmetic averages with respect to two polymers to estimate composition distribution indices. It becomes apparent that the M_w/M_n(block) values of blend **E**s are much larger than those of **NE**s, when Figure 2a is compared with Figure 2d.

The 3 mm thick, 75 mm diameter silicon wafers were rinsed in a strong oxidizing bath containing concentrated sulfuric acid and 30% hydrogen peroxide in a volume ratio of 7:3. Thin film specimens for reflectivity measurements were prepared by spin-coating dioxane solutions of the blend samples on the cleaned silicon wafers and annealed at 170 °C for 1 week. The solvent, dioxane, used for spin-coating is a common good solvent for the two component polymers, S and P. Actually, several thin films with different thicknesses were prepared for each sample, and then the best one without "islands" or "holes" formation was selected for subsequent neutron experiments by measuring X-ray reflectivity (XR) after thermal annealing. The thicknesses of all the thin film specimens were determined to be between 130 and 300 nm by XR measurements on the Rigaku instrument (Rigaku ATX-G).

Neutron reflectivity (NR) measurements were performed at two different pulsed neutron source laboratories. The CRISP at ISIS pulsed neutron source, at Rutherford Appleton Laboratory in the United Kingdom, was employed for measurements of specular reflectivities at three constant incident angles of the beam (θ = 0.25°, 0.65°, and 1.5°) against the film surface.[46] Subsequently, three profiles were connected and analyzed using Parratt's algorithm.[47] The ARISA reflectometer at the Neutron Science Laboratory, High Energy Accelerator Research Organization in Tsukuba,[48] was employed for additional measurements with θ = 0.35° and 0.8°. To obtain basic structural features of bulk states of the present copolymers, transmission electron microscopy (TEM) and small-angle X-ray scattering (SAXS) measurements were carried out for the thermally annealed bulk cast films from THF solutions of blends.[30]

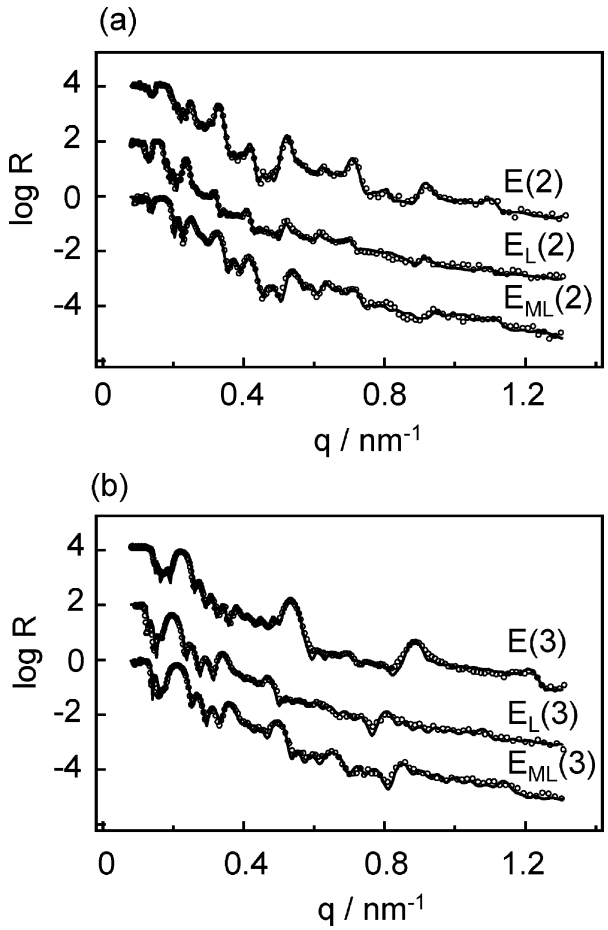

Figure 4. NR profiles of **E**s, $\mathbf{E_L}$s, and $\mathbf{E_{ML}}$s for the (a) diblock system and (b) triblock system. Horizontal axes represent the momentum transfer along the direction normal to the film surface, q, while vertical axes represent logarithmic reflectivity. The top profiles are for **E**s (**E(2)** and **E(3)**), the middle profiles are $\mathbf{E_L}$s ($\mathbf{E_L(2)}$ and $\mathbf{E_L(3)}$), and the bottom profiles are $\mathbf{E_{ML}}$s ($\mathbf{E_{ML}(2)}$ and $\mathbf{E_{ML}(3)}$). Open circles represent the measured reflectivities, while the solid lines show the calculated reflectivities.

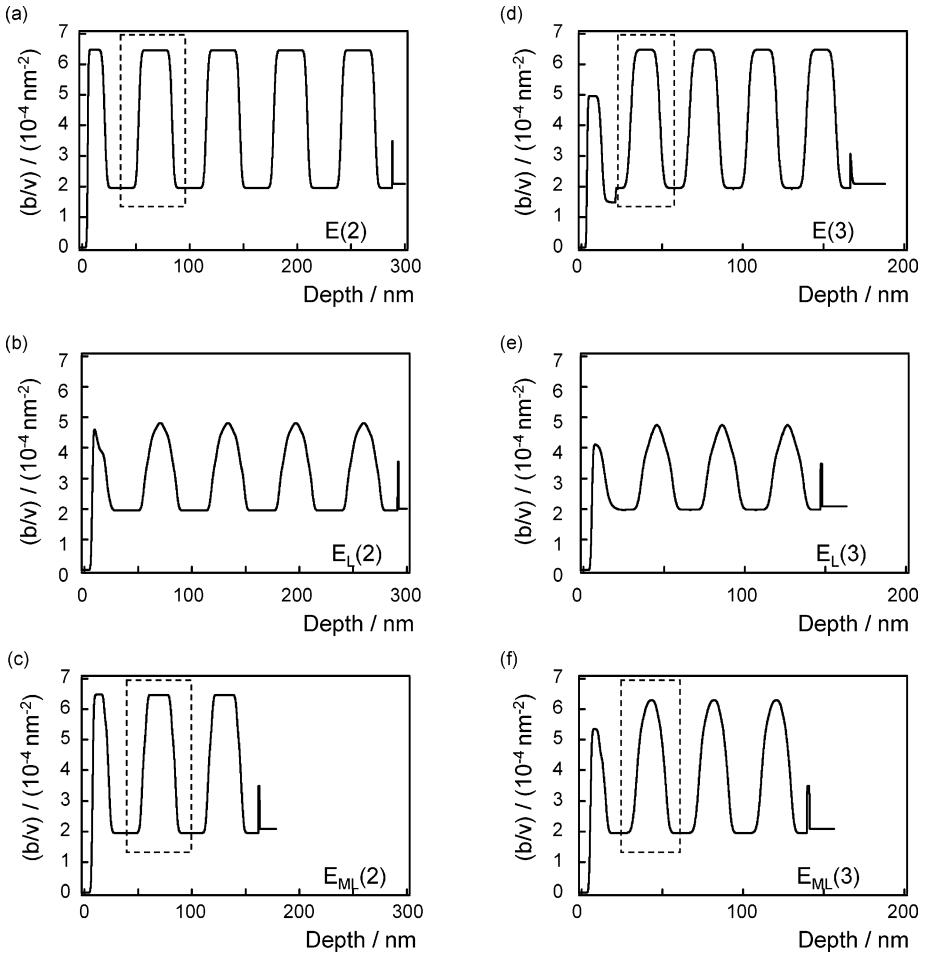

Figure 5. Scattering length density profiles along the depth direction for the films of the **E** series for reflectivity calculations: (a) **E(2)**, (b) $\mathbf{E_L(2)}$, (c) $\mathbf{E_{ML}(2)}$, (d) **E(3)**, (e) $\mathbf{E_L(3)}$, and (f) $\mathbf{E_{ML}(3)}$. The profiles in boxes drawn with dashed lines in (a), (c), (d), and (f) are analyzed in detail in Figure 8.

Results

Figure 3 compares typical examples of TEM images for diblock and triblock systems in bulk. Figure 3a indicates **E(2)** and Figure 3b indicates **E(3)**, which have relatively larger M_w/M_n(block) values. These show simple and homogeneous lamellar structures with flat interfaces. SAXS profiles for bulk films of all blends show integer-ordered diffraction peaks, indicating that simple lamellar microdomain structures are formed by monodispersed molecules in molecular weights but heterogeneous in composition (diffraction patterns are not shown here). Lamellar domain spacing, D, can be evaluated according to Bragg's relationship, $|q_p| = 2\pi/D$, between the magnitude of the scattering vector where diffracted peaks are located, $|q_p|$, and domain spacing, D. Estimated values are listed in Table 3. These data may provide useful references for structural characteristics of thin films, which are the principal objectives of this work. It is apparent that the D values of the triblock system are considerably smaller than those of the corresponding diblock system, though the molecular weights of the members of the triblock system are slightly larger than those of the diblock system. This is expected from a structural viewpoint since the domain sizes of triblock copolymers are identical to those of the diblock copolymers which have half of the molecular weight of the triblock copolymers.[12,49]

Figure 4a,b provides a comparison of the NR profiles from **E**s, $\mathbf{E_L}$s, and $\mathbf{E_{ML}}$s for the diblock and triblock systems. The vertical axes represent logarithmic reflectivities, and horizontal axes represent the magnitude of the momentum transfer along the direction normal to the film surface $|q|$ ($= 4\pi \sin\theta/\lambda$), where λ is the wavelength. Bragg peaks in reflectivity profiles for $\mathbf{E_L}$ and $\mathbf{E_{ML}}$ blends in Figure 4a,b are fairly weak, especially for the higher q region, indicating that the densities of the labeled segments are not very high for these blends. In Figure 4, the open circles indicate measured reflectivities and are well fitted with the calculated solid lines using scattering length density (b/v) profiles along the depth direction of the thin films as displayed in Figure 5, which serves to validate the b/v profiles in Figure 5. The b/v profiles for **E**s in Figure 5a,d reveal that the PS-d_8 lamellae with a b/v value of 6.47×10^{-4} nm^{-2} and the P2VP lamellae with a value of 1.95×10^{-4} nm^{-2} are stacked alternately in parallel with the silicon surface of the thin film. Block chains with different lengths in blend **E**s appear to be well mixed into one homogeneous lamellar microdomain. A typical example, shown in Figure 5a, indicates that a lamella of the PS-d_8 phase whose thickness is approximately one-half of that of the regular PS lamella is located at the top of the film as a result of the lower surface energy of PS relative to P2VP. On the other hand, a lamella of the P2VP phase is set at the bottom of the film because of higher affinity with the SiO_X layer whose thickness is ~1.5 nm.

Blend samples of $\mathbf{E_L}$s and $\mathbf{E_{ML}}$s have almost the same composition, molecular weight, and composition distribution as **E**s. It is thus expected that a consistent microdomain must be formed. However, fairly different density profiles relative to those of perdeuterated **E**s blends have been observed for $\mathbf{E_L}$s and $\mathbf{E_{ML}}$s in Figure 5 because of the coexistence of PS-h_8 block

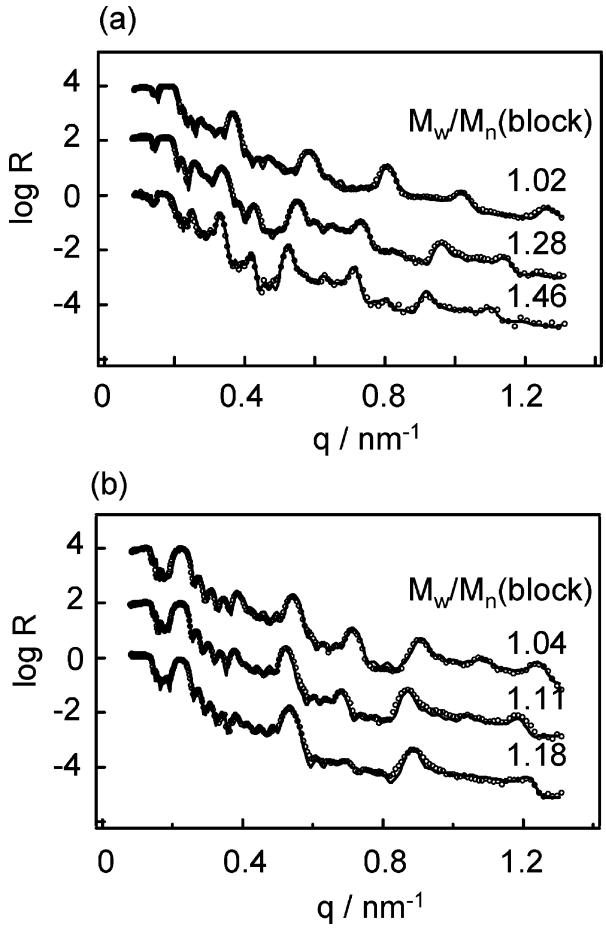

Figure 6. NR profiles of perdeuterated blends for (a) the diblock system and (b) the triblock system. The top profiles are for pure block copolymers, DP-55 and PDP-55, the middle profiles are for **NE**s (**NE(2)** and **NE(3)**), and the bottom profiles are for **E**s (**E(2)** and **E(3)**). The curves are displayed in order of the magnitude of composition distribution indices from top to bottom. Open circles highlight the measured reflectivities, and the solid lines highlight the calculated reflectivities.

chains in the PS phase, whose b/v value is 1.41×10^{-4} nm^{-2}. From Figure 5b,e it is apparent that deuterated segments of the longer chains are localized broadly with peaks at the center of the lamellar domains, while it is difficult to recognize the segmental distribution of the unlabeled short chains from b/v profiles in Figure 5c,f. This issue will be discussed in more detail below. D values were determined from b/v profiles and are also listed in Table 3.

The NR profiles of perdeuterated parent copolymers and their blends for both diblock and triblock systems are compared in Figure 6. Profiles for the diblock system are shown in Figure 6a, while those of the triblock system are shown in Figure 6b. The top profiles are for simple parent block copolymers, DP-55 and PDP-55 as references. The remaining reflectivity profiles are arranged with respect to the order of the magnitude of M_w/M_n(block) from top to bottom (reference block copolymers, **NE**s and **E**s). Two reflectivity profiles are displayed for each blend: one for measured reflectivities shown as open circles and one representing calculated reflectivities depicted as solid lines. The latter were obtained using scattering length density profiles along the depth direction of the thin films, as displayed in Figure 7. The experimental data are all well-fitted with the calculated lines in Figure 6, showing that the PS-d_8 and P2VP lamellae are stacked alternately parallel to the silicon surface in these thin films. The total domain spacing, D, estimated from b/v profiles in Figure 7 is listed in Table 3. From this table, it is readily seen that the microdomain repeating distances in thin films are similar to those observed in bulk films. This indicates that equilibrium structures have been formed due to annealing in both films.

The interfacial thicknesses between PS and P2VP lamellae, $t_I = 1/(d\phi_i(z)/dz)_{\phi_i=0.5}$, defined as the inverse of the tangential slope at the middle point in the interfacial profiles, were also evaluated, and the obtained values are listed in Table 3. The interfacial thicknesses of the parent block copolymers, DP-55 and PDP-55, are 3.3 and 3.2 nm, respectively, and in good agreement with the results of our latest investigations on DP and PDP[50] while not with those of the other previous works on the same polymer system.[42,51,52] The discrepancy in the evaluated interfacial thickness among those studies may be attributed to the difference in sample preparation of thin film specimens. In the previous studies toluene was used for spin-coating, which is not a good solvent for P2VP. Once the nonequilibrium factor is introduced into a thin film, it cannot be removed easily and perfectly by thermal annealing during short period of time even at high temperature. On the other hand, t_I for **NE**s and **E**s are 3.8 and 4.0 nm, respectively, for both diblock and triblock systems. These measurements are meaningfully larger than those of monodispersed parent block copolymers. Thus, it has been clarified that the interfacial thickness depends on the block chain length distribution and will be further discussed below.

Discussion

We first discuss the localization phenomena of short and long chains. These blend samples were prepared from two labeled block copolymers and one unlabeled block copolymer with a short PS block, for the purpose of indirect observation of the segmental distribution of the short block chain. For extraction of the segmental distribution of unlabeled chains in the microdomain, it is necessary to assume incompressibility as is expressed in eq 1 and additivity in b/v as is shown in eq 2

$$\sum \phi_i(z) = 1 \tag{1}$$

$$(b/v)(z) = \sum (b/v)_i \phi_i(z) \tag{2}$$

where $(b/v)_i$ and $\phi_i(z)$ are the b/v value of i component (i denotes PS-d_8, PS-h_8, or P2VP) and its volume fraction at distance z along depth direction from the thin film surface, respectively. The value of $\phi_{P2VP}(z)$ in the PS phase and both $\phi_{PS-d_8}(z)$ and $\phi_{PS-h_8}(z)$ in the P2VP phase are assumed to be zero, since the PS and P2VP phases separate in the strong segregation regime. At the lamellar interfaces of $\mathbf{E_{ML}}$s, the segmental distributions of PS (containing both PS-d_8 and PS-h_8) or P2VP were assumed to be described by error functions as in the case for **E**s, since **E**s and $\mathbf{E_{ML}}$s should have essentially the same structures and interfacial profiles. Figure 8a,b compares the volume fraction profiles. It should be noted that the vertical axes represent the polystyrene volume fraction ϕ_S instead of b/v. The solid lines representing short chains were derived by subtraction of the contribution of the middle and the long chains represented by b/v profiles within boxes drawn as dashed lines in Figure 5c,f (also expressed as dotted lines in Figure 8a,b to distinguish from the polystyrene chains designated in boxes drawn as dashed lines in Figure 5a,d and represented by the broken lines in Figure 8a,b, respectively). Both parts a and b of Figure 8 clearly reveal the localization behavior of short chains near the domain interface. In accord with the results of Figures 5 and 8, the corresponding chain distributions in the microdomain are

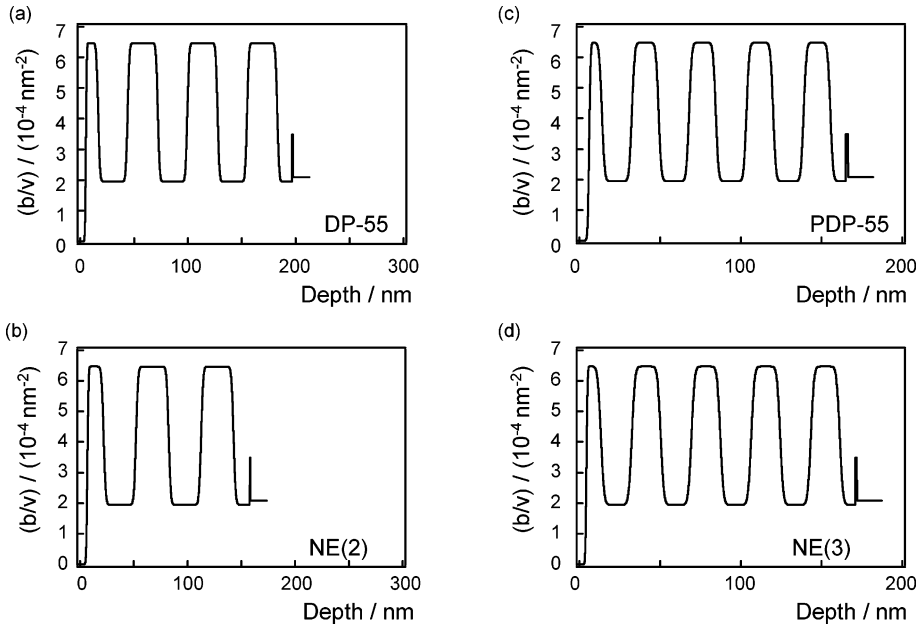

Figure 7. Scattering length density profiles along the depth direction for the films of perdeuterated blends used for reflectivity calculations: (a) DP-55, (b) **NE(2)**, (c) PDP-55, and (d) **NE(3)**.

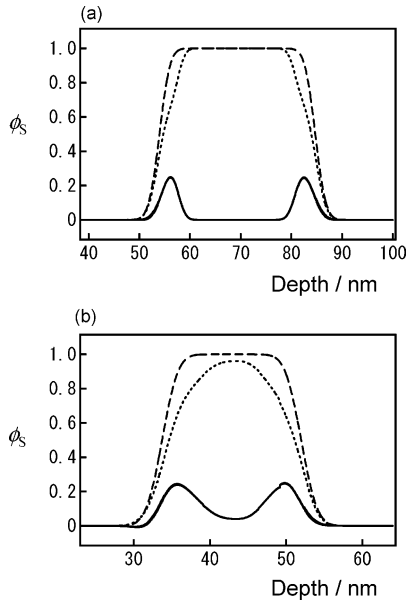

Figure 8. Estimation of segmental distributions of short polystyrene chains in lamellar domains: (a) diblock system; (b) triblock system. The broken lines denote perdeuterated blends **E(2)** and **E(3)**. The corresponding areas are surrounded by dashed boxes in Figure 5a,d, while the dotted lines indicate selectively labeled blends of $\mathbf{E_{ML}(2)}$ and $\mathbf{E_{ML}(3)}$. These areas are boxed in Figure 5c,f. The solid lines for unlabeled short polystyrene chains are estimated by subtraction of dotted lines from broken lines. Horizontal axes are depths from film surface while the vertical axes are volume fractions.

schematically drawn in Figure 9, where the localization of short chains in the vicinity of the domain interface and the localization of long chains at the domain center are both evident. The localization phenomena of thin films in polydispersed systems evidenced by these experiments are quite consistent with results obtained by transmission electron microscopy and small-angle X-ray scattering for bulk films having similar polydispersities.[28−30] The observations of ordered binary block copolymer mixtures by Mayes et al. provide additional supporting evidence.[26]

Next, we discuss the composition distribution dependence of interfacial thickness. Table 3 indicates that interfacial thickness

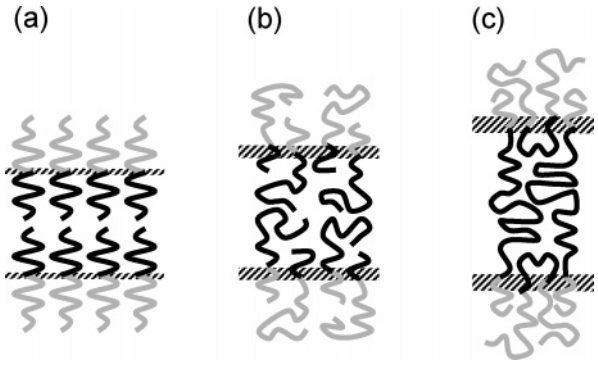

Figure 9. Schematic comparison of three different domain structures: (a) monodispersed diblock system, (b) polydispersed diblock system, and (c) polydispersed triblock system.

increases with an increase in the M_w/M_n(block) value for the diblock and triblock systems. To gain a further understanding of this phenomenon in a more quantitative sense, interfacial thicknesses for the blends having high M_w/M_n(block) values were normalized to those of monodispersed parent copolymers ($t_{I,0}$): $t_{I(DP-55)}$ for the diblock system and $t_{I(PDP-55)}$ for the triblock system. The normalized thickness values $t_I/t_{I,0}$ have been plotted against M_w/M_n(block) values in Figure 10. It is clear from Figure 10 that (i) interfacial thicknesses increase with increasing composition distribution indices for both systems and that (ii) the incremental increase for the triblock system is larger than that of the diblock system. However, the absolute incremental increase of the interfacial thickness is relatively small for both systems.

The apparent thickness, evaluated by NR, for polymer interface is usually much larger than the prediction of the mean-field theory, and this discrepancy can be quantitatively explained by introducing the concept of thermal capillary wave on polymer interface.[50,53,54] According to the concept of capillary wave, its contribution to interfacial broadening is inversely proportional to the magnitude of interfacial tension. Though interfacial tension cannot be exactly evaluated for the polydispersed block copolymer system studied here, it was calculated by the mean-field theory for a bimodal block copolymer blend by Shi and

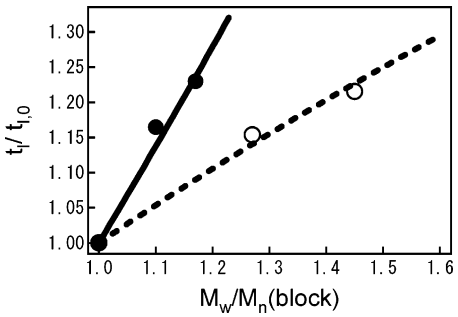

Figure 10. Composition distribution dependence of the reduced interfacial thickness, $t_l/t_{l,0}$, for both diblock and triblock systems. Interfacial thicknesses for monodispersed copolymers of 3.3 nm for DP-55 and 3.2 nm for PDP-55 were chosen as reference $t_{l,0}$ values. The open circles represent the diblock system, while the filled circles represent the triblock system. The broken and the solid lines are drawn as guides for two systems.

Noolandi[44] and for a homopolymer blend with polydispersity by Broseta et al.[45] The latter work reported that short chains in the polydispersed system lower effective interfacial tension due to their existence at the interface. This result suggests that the decrease in interfacial tension due to polydispersity could cause interfacial broadining by thermal capillary wave, and hence it is thought that the apparent interfacial thickness of the polydispersed system is broader than that of monodispersed system as determined by NR measurements.

The AB diblock copolymer has one junction point per molecule and retains a tail conformation, while the BAB triblock copolymer possesses two junction points and adopts loop and bridge conformations in bulk; therefore, the degree of freedom of the middle chain in the BAB triblock copolymer is suppressed. It is conceivable that the constraint effect for middle short and long chains could be enhanced for the triblock system. This leads to the larger distribution of junction points of the BAB triblock copolymer than that of the AB diblock copolymer along the normal to lamellar interface, and a larger increment of interfacial thickness is attained for the BAB triblock copolymer system.

In conclusion, we have found that (1) all blend samples with various M_w/M_n(block) values with composition ratios near 0.5/0.5 form uniform lamellar structures both in thin film and in bulk and (2) the localization phenomena of longer and shorter block chains in uniform domains consisting of block chains with various lengths were observed directly by neutron reflectivity measurements. Segments of longer block chains are localized broadly at the center of domains while segments of the shorter block chains are localized near the domain interface. It has also been clarified that (3) interfacial thickness as well as domain spacing increases with an increase in composition distribution index for both AB diblock and BAB triblock systems. Furthermore, (4) the incremental interfacial thickness for the BAB triblock system is larger than that of the AB diblock system, but indicating that the miscibility effects of polydispersity for both systems are very small.

Acknowledgment. A.N. thanks JSPS Research Fellowships for Young Scientists (No. 18-6533). The authors also thank Dr. S. Arai of the Nagoya University EcoTopia Science Institute for assistance with transmission electron micrograph measurements, Dr. J. Suzuki at the Computing Research Center in High Energy Accelerator Research Organization, and Mr. T. Hikage at the High Intensity X-ray Diffraction Laboratory of Nagoya University for assistance with X-ray measurements. The NR experiments were performed under funding from the Japan−UK Collaboration Program on Neutron Scattering supported by a Grant-in-Aid for Creative Scientific Research (No. 16GS0417) from the Ministry of Education, Culture, Sports, Science and Technology of Japan. The authors also thank Dr. R. Dalgliesh at Rutherford Appleton Laboratory for his kind assistance with NR experiments and Dr. M. Harada at Toyota Inc. Central R&D Laboratories for assistance with analysis of NR data. This work was supported by funding from the 21st century COE Program entitled "The Creation of Nature Guided Materials Processing".

References and Notes

(1) Matsuo, M.; Sagae, S.; Asai, H. *Polymer* **1969**, *10*, 79−87.
(2) Molau, G. E. In *Block Polymers*; Aggarwal, S. L., Ed.; Plenum: New York, 1970; p 79.
(3) Inoue, T.; Soen, T.; Hashimoto, T.; Kawai, H. *J. Polym. Sci., Part A-2* **1969**, *7*, 1283−1302.
(4) Hashimoto, T.; Shibayama, M.; Kawai, H. *Macromolecules* **1980**, *13*, 1237−1247.
(5) Matsushita, Y.; Mori, K.; Saguchi, R.; Nakao, Y.; Noda, I.; Nagasawa, M. *Macromolecules* **1990**, *23*, 4313−4317.
(6) Helfand, E.; Wasserman, Z. R. *Macromolecules* **1976**, *9*, 879−888.
(7) Leibler, L. *Macromolecules* **1980**, *13*, 1602−1617.
(8) Semenov, A. N. *Macromolecules* **1993**, *26*, 6617−6621.
(9) Ohta, T.; Kawasaki, K. *Macromolecules* **1986**, *19*, 2621−2632.
(10) Matsushita, Y. *J. Polym. Sci., Part B* **2000**, *38*, 1645−1655.
(11) Miwa, Y.; Yamamoto, K.; Sakaguchi, M.; Sakai, M.; Tanida, K.; Hara, S.; Okamoto, S.; Shimada, S. *Macromolecules* **2004**, *37*, 831−839.
(12) Matsushita, Y.; Nomura, M.; Watanabe, J.; Mogi, Y.; Noda, I.; Imai, M. *Macromolecules* **1995**, *28*, 6007−6013.
(13) Takano, A.; Kadoi, O.; Hirahara, K.; Kawahara, S.; Isono, Y.; Suzuki, J.; Matsushita, Y. *Macromolecules* **2003**, *36*, 3045−3050.
(14) Matsushita, Y.; Iwata, H.; Asari, T.; Uchida, T.; ten Brinke, G.; Takano, A. *J. Chem. Phys.* **2004**, *121*, 1129−1132.
(15) Mogi, Y.; Kotsuji, H.; Kaneko, Y.; Mori, K.; Matsushita, Y.; Noda, I. *Macromolecules* **1992**, *25*, 5408−5411.
(16) Takano, A.; Wada, S.; Sato, S.; Araki, T.; Hirahara, K.; Kazama, T.; Kawahara, S.; Isono, Y.; Ohno, A.; Tanaka, N.; Matsushita, Y. *Macromolecules* **2004**, *37*, 9941−9946.
(17) Takano, A.; Kamaya, I.; Takahashi, Y.; Matsushita, Y. *Macromolecules* **2005**, *38*, 9718−9723.
(18) Karatasos, K.; Anastasiadis, S. H.; Pakula, T.; Watanabe, H. *Macromolecules* **2000**, *33*, 523−541.
(19) Tanaka, H.; Hasegawa, H.; Hashimoto, T. *Macromolecules* **1991**, *24*, 240−251.
(20) Mayes, A. M.; Russell, T. P.; Satija, S. K.; Majkrzak, C. F. *Macromolecules* **1992**, *25*, 6523−6531.
(21) Matsushita, Y.; Torikai, N.; Mogi, Y.; Noda, I.; Han, C. C. *Macromolecules* **1993**, *26*, 6346−6349.
(22) Torikai, N.; Takabayashi, N.; Noda, I.; Koizumi, S.; Mori, Y.; Matsushita, Y. *Macromolecules* **1997**, *30*, 5698−5703.
(23) Hashimoto, T.; Yamasaki, K.; Koizumi, S.; Hasegawa, H. *Macromolecules* **1993**, *26*, 2895−2904.
(24) Court, F.; Hashimoto, T. *Macromolecules* **2001**, *34*, 2536−2545.
(25) Koneripalli, N.; Levicky, R.; Bates, F. S.; Matsen, M. W.; Satija, S. K.; Ankner, J.; Kaiser, H. *Macromolecules* **1998**, *31*, 3498−3508.
(26) Mayes, A. M.; Russell, T. P.; Deline, V. R.; Satija, S. K.; Majkrzak, C. F. *Macromolecules* **1994**, *27*, 7447−7453.
(27) Bendejacq, D.; Ponsinet, V.; Joanicot, M.; Loo, Y.-L.; Register, R. A. *Macromolecules* **2002**, *35*, 6645−6649.
(28) Matsushita, Y.; Noro, A.; Iinuma, M.; Suzuki, J.; Ohtani, H.; Takano, A.; Matsushita, Y. *Macromolecules* **2003**, *36*, 8074−8077.
(29) Noro, A.; Iinuma, M.; Suzuki, J.; Takano, A.; Matsushita, Y. *Macromolecules* **2004**, *37*, 3804−3808.
(30) Noro, A.; Cho, D.; Takano, A.; Matsushita, Y. *Macromolecules* **2005**, *38*, 4371−4376.
(31) Cho, D.; Noro, A.; Takano, A.; Matsushita, Y. *Macromolecules* **2005**, *38*, 3033−3036.
(32) Burger, C.; Ruland, W.; Semenov, A. N. *Macromolecules* **1990**, *23*, 3339−3346.
(33) Sides, S. W.; Fredrickson, G. H. *J. Chem. Phys.* **2004**, *121*, 4974−4986.
(34) Lynd, N. A.; Hillmyer, M. A. *Macromolecules* **2005**, *38*, 8803−8810.
(35) Jiang, Y.; Chen, T.; Ye, F.; Liang, H.; Shi, A.-C. *Macromolecules* **2005**, *38*, 6710−6717.
(36) Martinez-Veracoechea, F. J.; Escobdo, F. A. *Macromolecules* **2005**, *38*, 8522−8531.
(37) Jiang, Y.; Huang, R.; Liang, H. *J. Chem. Phys.* **2005**, *123*, 124906.
(38) Jiang, Y.; Yan, X.; Liang, H.; Shi, A.-C. *J. Phys. Chem. B* **2005**, *109*, 21047−21055.

(39) Li, X.; Tang, P.; Qiu, F.; Zhang, H.; Yang, Y. *J. Phys. Chem. B* **2006**, *110*, 2024−2030.
(40) Anastasiadis, S. H.; Russell, T. P.; Satija, S. K.; Majkrzak, C. F. *J. Chem. Phys.* **1990**, *92*, 5677−5691.
(41) Mayes, A. M.; Johnson, R. D.; Russell, T. P.; Smith, S. D.; Satija, S. K.; Majkrzak, C. F. *Macromolecules* **1993**, *26*, 1047−1052.
(42) Torikai, N.; Noda, I.; Karim, A.; Satija, S. K.; Han, C. C.; Matsushita, Y.; Kawakatsu, T. *Macromolecules* **1997**, *30*, 2907−2914.
(43) Torikai, N.; Matsushita, Y.; Noda, I.; Karim, A.; Satija, S. K.; Han, C. C. *Physica B* **1995**, *213&214*, 694−696.
(44) Shi, A.-C.; Noolandi, J. *Macromolecules* **1994**, *27*, 2936−2944.
(45) Broseta, D.; Fredrickson, G. H.; Helfand, E.; Leibler, L. *Macromolecules* **1990**, *23*, 132−139.
(46) Harada, M.; Suzuki, T.; Ohya, M.; Kawaguchi, D.; Takano, A.; Matsushita, Y.; Torikai, N. *J. Polym. Sci., Part B* **2005**, *43*, 1486−1494.
(47) Parratt, L. G. *Phys. Rev.* **1954**, *95*, 359-.
(48) Torikai, N.; Furusaki, M.; Matsuoka, H.; Matsushita, Y.; Shibayama, M.; Takahara, A.; Takeda, M.; Tasaki, S.; Yamaoka, H. *Appl. Phys. A* **2002**, *74*, S264−S266.
(49) Hadziioannou, G.; Skoulios, A. *Macromolecules* **1982**, *15*, 258−262.
(50) Torikai, N.; Matsushita, Y.; Langridge, S.; Bucknall, D.; Penfold, J.; Takeda, M. *Physica B* **2000**, *283*, 12−16.
(51) Anastasiadis, S. H.; Retsos, H.; Toprakcioglu, C.; Menelle, A.; Hadziioannou, G. *Macromolecules* **1998**, *31*, 6600−6604.
(52) de Jeu, W. H.; Lambooy, P.; Hamley, I. W.; Vaknin, D.; Pedersen, J. S.; Kjaer, K.; Seyger, R.; van Hutten, P.; Hadziioannou, G. *J. Phys. II* **1993**, *3*, 139−146.
(53) Shull, K. R.; Mayes, A. M.; Russell, T. P. *Macromolecules* **1993**, *26*, 3929−3936.
(54) Sferrazza, M.; Xiao, C.; Jones, R. A. L.; Bucknall, D. G.; Webster, J.; Penfold, J. *Phys. Rev. Lett.* **1997**, *78*, 3693−3696.

MA061487K